

Convective Heat Transfer over a Wall Mounted Cube Using Large Eddy Simulation

Habibollah heidarzadeh, Mousa farhadi^C and Kurosh sedighi

*Department of thermo fluids, Faculty of Mechanical Engineering
Babol University of Technology, IRAN*

Received: 16/01/2011 – Revised 10/05/2012 – Accepted 13/05/2012

Abstract

Fluid flow and convective heat transfer over wall mounted cube have been studied numerically using Large Eddy Simulation. Surface of wall mounted cube and plane floor has a constant heat flux. Two subgrid scale models were used in this study; Wall-Adapting Eddy viscosity (WALE) and Dynamic Smagorinsky (DS). The numerical results were compared with the experimental data of Nakamura et al [2] that showed DS model has better results toward WALE model. Results contain the plots of time averaged normalized streamwise velocity and Reynolds stress in different positions, Temperature contours, local Nusselt number over the surfaces of cube and some characteristics of flow field and heat transfer. The local convective heat transfer from the surfaces of the cube and plate are directly related to the complexity of flow field.

Keywords: wall mounted cube; large eddy simulation; turbulent flow; WALE model; Dynamic Smagorinsky model; heat transfer

1. Introduction

Flow around a three dimensional obstacle is a great interest in engineering applications such as the computation of wind loads on buildings, simulation of the flow around vehicles and air cooling of the electronic boards. Flow over wall mounted obstacles; generate complex phenomena such as flow separation, partial reattachment, vortex shedding, high turbulence level and large-scale turbulent structures. The *RANS* (Reynolds Averaged Navier Stockes) methods are not suitable for predicting such flow but Direct Numerical Solution (*DNS*) and Large Eddy Simulation (*LES*) are clearly more suitable methods [1].

Most previous research on wall mounted cube was considered internal flow around the cube in a channel. As heat transfer and fluid flow characteristics are changed in external flow, Nakamura *et al* [2] investigated external flow around cubic obstacle. They studied the fluid flow and local heat transfer around a wall mounted cube on a flat plate turbulent boundary layers. They studied the effect of flow pattern such as vortex shedding, flow separation and flow reattachment on the convective heat transfer. On the other work, Nakamura *et al.* [3] experimentally studied the fluid flow and local heat transfer around a wall mounted cube at 45 degree to the flow on a flat plate turbulent boundary layers. Sohankar[4] studied numerically flow over a square-section cylinder

^C Corresponding Author: M. Farhadi

Email: mfarhadi@nit.ac.ir Telephone: +98 1113232071

Fax: P.O. Box 484

© 2009-2012 All rights reserved. ISSR Journals

PII: S2180-1363(10)4280-X

from moderate to high Reynolds number using large eddy simulation. Detailed information was obtained about the flow field that was studied with the instantaneous and the mean quantities such as pressure, turbulent stresses, turbulent kinetic energy, vortices and etc. Their results indicated that the effect of Reynolds number on the global quantities, the mean and the large scale instantaneous flow structures is not much at the higher Reynolds numbers.

The concept of flow over a wall mounted cube in a channel is extensively discussed by different researchers. Niceno *et al.* [5] numerically studied the dynamics of flow and heat transfer on an internally heated multilayered matrix of cubes mounted on one of the walls of a plane channel using *LES*. Detailed information was obtained about the instantaneous and averaged velocity and temperature in the fluid around the cube, as well as the temperature and heat transfer on the cube surfaces. In addition, the simulation provided a detailed about to the vortical structure and turbulence field around the cube and their relationship with the cube surface heat transfer. Krajnovic and Davidson [6] and Farhadi and Rahnama [7] showed the structure of vortices around the cube with the Second Invariant technique for Reynolds number 40000. Recently, Hwang and Yang [8] have studied the vortical structures of flow around a wall mounted cube in a channel at low to moderate Reynolds numbers up to 3500 using the Direct Numerical Simulation (*DNS*). Their results showed that as the Reynolds number increases, the structure of the horseshoe vortex system becomes complex, and the number of vortices increases in pairs. Farhadi and Sedighi [9] studied Reynolds number effects on flow over a wall mounted cube in a channel. Lammers *et al.* [10] investigated a turbulent channel flow, with regularly spaced two dimensional roughness elements mounted at the wall and perpendicular to the flow direction. They studied on the effect of elements mounted at the wall on the streamwise and the spanwise velocity fluctuation snear the wall. Some of authors e.g. Bakis and Bakis *et al.* [11-12] studied on other three dimensional prism e.g. sphere. They investigated experimentally on a flow around a sphere. Also Chakrabarty and Brahma [13] studied experimentally effect of wall proximity in fluid flow and heat transfer from a square prism placed inside a wind tunnel. Their results showed that the values of average Nusselt number for all angles of attack, Reynolds numbers, and blockage ratios decreases as the prism moves in the direction of the upper wall of the wind tunnel.

In present study flow structure and heat transfer over a wall mounted cube on a flat plate in the turbulent boundary layers were investigated numerically. Numerical simulation is done using large eddy simulation (*LES*) method with two subgrid scale models. Complex phenomena is shown using time averaged streamlines on symmetry plane ($z=0$) and plate ($y=0$) and its effect over the fluid flow characteristics, local and average convective heat transfers.

2. Numerical details

2.1. Governing equations

Turbulent flow over obstacle is modeled by *LES* in which the larger three dimensional unsteady turbulent motions are directly represented, whereas the effect of small scales of motion is modeled. To do this, a filtering operation is introduced to decompose the velocity vector, u_i into the sum of a filtered (or resolved) component, \bar{u}_i and a residual (or subgrid scale (*SGS*)) component u'_i . This operation can be represented with a filter of width Δx such that convolution of any quantity $f(x_i, t)$ by the filter function $G_{\Delta x}(x_i)$ is in the form eq. (1).

$$\bar{f}(x_i, t) = \int \bar{f}(y_i, t) G_{\Delta x}(x_i)(x_i - y_i) dy_i, \quad f' = f - \bar{f} \quad (1)$$

The equations for the evolution of the filtered velocity filed are derived from the Navier–Stokes equations. These equations are of the standard form, with the momentum equation containing the residual stress tensor. Application of the filtering operation to the continuity and Navier–Stokes equations give the resolved Navier–Stokes equations, which, in non-dimensional incompressible form, are equations (2), (3) and (4).

$$\frac{\partial \bar{u}_i}{\partial x_i} = 0 \quad (2)$$

$$\frac{\partial \bar{u}_i}{\partial t} + \frac{\partial}{\partial x_j} (\bar{u}_i \bar{u}_j) = -\frac{1}{\rho} \frac{\partial \bar{p}}{\partial x_i} + \nu \frac{\partial^2 \bar{u}_i}{\partial x_j \partial x_j} - \frac{\partial \tau_{ij}}{\partial x_j} \quad (3)$$

$$\frac{\partial \bar{T}}{\partial t} + \frac{\partial (\bar{u}_i \bar{T})}{\partial x_i} = \frac{\partial}{\partial x_j} \left(\alpha \frac{\partial \bar{T}}{\partial x_j} - h_j \right) \quad (4)$$

where \bar{P} is the pressure, and \bar{u}_1, \bar{u}_2 and \bar{u}_3 are the streamwise, cross-stream, and spanwise components of velocity, respectively. These govern the dynamics of the large, energy-carrying scales of motion. Reynolds number is defined as, $U_{inlet}H/\nu$ where U_{inlet} and H are the inlet velocity of entrance profile and cube height, respectively. The effect of small scales upon the resolved part of turbulence appears in the *SGS* stress term as eq. (5):

$$\tau_{ij} = \overline{u_i u_j} - \bar{u}_i \bar{u}_j \quad (5)$$

which must be modeled. The main effect of the *SGS* stresses is dissipative around the cut-off spectrum, i.e. to withdraw energy from the part of the spectrum that can be resolved. One model for the *SGS* stress term τ_{ij} is based on its dependence on the filtered strain rate through an eddy viscosity given by eq. (6).

$$\tau_{ij} = 2\nu_{SGS} \bar{S}_{ij} + \frac{1}{3} \tau_{kk} \delta_{ij} \quad (6)$$

where \bar{S}_{ij} is the resolved strain rate given by eq. (7).

$$\bar{S}_{ij} = \frac{1}{2} \left(\frac{\partial \bar{u}_i}{\partial x_j} + \frac{\partial \bar{u}_j}{\partial x_i} \right) \quad (7)$$

where ν_{SGS} is the *SGS* eddy-viscosity.

The modified *SGS* heat fluxes h_j are defined as:

$$h_j = \overline{u_j T} - \bar{u}_j \bar{T} \quad (8)$$

The modified *SGS* heat fluxes h_j are modeled by the eddy-diffusivity hypothesis with constant turbulent Prandtl number, Pr_t as eq. (9).

$$h_j = -\frac{\nu_{SGS}}{Pr_t} \frac{\partial \bar{T}}{\partial x_j} \quad (9)$$

In this study, we have $Pr_t = 0.85$.

2.2. Subgrid scale model

In this study, we used two subgrid scale models for modeling of *SGS* eddy viscosity. These two models are: 1. *WALE* (wall-adapting local eddy viscosity) and 2. *DS* (Dynamic Smagorinsky).

2.2.1 *WALE* (wall-adapting local eddy viscosity) model

The *WALE* (wall-adapting local eddy viscosity) model by Nicoud and Ducros [14] was used to model the *SGS* eddy-viscosity as eq. (10).

$$\nu_{SGS} = L_s^2 \frac{\left(\zeta_{ij} \zeta_{ij} \right)^{\frac{3}{2}}}{\left(\bar{S}_{ij} \bar{S}_{ij} \right)^{\frac{5}{2}} + \left(\zeta_{ij} \zeta_{ij} \right)^{\frac{5}{4}}} \quad (10)$$

where L_s is a length scale given by eq. (11)

$$L_s = \min \left(Kr, C_w V^{\frac{1}{3}} \right) \quad (11)$$

K is von Karman's constant, r is the normal distance to the closest wall, V is the volume of the computational cell and ζ_{ij} is the traceless symmetric part of the square of the velocity gradient tensor defined as eq. (12).

$$\zeta_{ij} = \frac{1}{2} \left(\frac{\partial \bar{u}_i}{\partial x_k} \frac{\partial \bar{u}_k}{\partial x_j} + \frac{\partial \bar{u}_j}{\partial x_k} \frac{\partial \bar{u}_k}{\partial x_i} \right) - \frac{1}{3} \delta_{ij} \frac{\partial \bar{u}_l}{\partial x_k} \frac{\partial \bar{u}_k}{\partial x_l} \quad (12)$$

In this study, value of the *WALE* constant $C_w=0.325$. In both two *SGS* models $K = 0.4187$.

2.1.2 DS (Dynamic Smagorinsky) model

This model was first proposed by Smagorinsky .In this model, the eddy viscosity is modeled by eq. (13)

$$\nu_{SGS} = L_s^2 |\bar{S}| \quad (13)$$

where L_s is the mixing length for subgrid scales and $|\bar{S}|$ is given by eq. (14)

$$|\bar{S}| = \sqrt{2 \bar{S}_{ij} \bar{S}_{ij}} \quad (14)$$

L_s is computed using eq. (15)

$$L_s = \min \left(Kr, C_s V^{\frac{1}{3}} \right) \quad (15)$$

C_s is the Smagorinsky constant. In the Smagorinsky model, C_s value usually is around 0.1 but Germano et al. [15] and subsequently Lilly [16] conceived a procedure in which the Smagorinsky model constant, C_s , is dynamically computed based on the information provided by the resolved scales of motion. The dynamic procedure thus obviates the need for users to specify the model constant C_s in advance. The C_s is obtained using the dynamic Smagorinsky model varies in time and space over a fairly wide range.

2.3. Boundary conditions

In this study, the commercial *CFD* software FLUENT 6.3 was used for simulation that based on finite volume method. Associated pre-processor GAMBIT 2.2 was used for the construction of the computational grid. FLUENT uses a control-volume-based technique to convert a general scalar transport equation to an algebraic equation that can be solved numerically. This control volume technique consists of integrating the general scalar transport equation about each control volume that yields a discrete equation on each control-volume. In this software, pressure-based solver was used to solve discrete equations. The pressure-based solver uses a solution algorithm where the governing equations are solved sequentially and segregated from one another. Because the governing equations are non-linear and coupled, the solution loop must be carried out iteratively in order to obtain a converged numerical solution.

An important issue in the *LES* computations is that using at least second orders accuracy of both time and spatial discretization of the equations .Linear equations system that was yielded from discretization of equations was solved by using an implicit linear equation solver (Gauss-Seidel) in conjunction with an algebraic multi-grid (*AMG*) method. *SIMPLE* (semi implicit method for pressure linked equation) algorithm was used for coupling the pressure and velocity terms. Second-order-accurate Bounded Central-Differencing scheme by Leonard [17] is used for

spatial discretization of convection terms in governing equations. The *QUICK* and Central-Differencing scheme has some deficiencies in comparison with the Bounded Central-Differencing scheme. Central-Differencing scheme often leads to unphysical oscillations in the solution fields and *QUICK* scheme has numerical dissipation. For spatial discretization of diffusion terms Central-Differencing scheme that is second-order accurate was used. A second-order implicit scheme was used for temporal discretization of governing equations and all equations solved by iterative time-advancement (*ITA*) method in a time step. The time step Δt was set to 2×10^{-3} s and kept constant during the simulation. The total time in the simulation was 15000 time steps.

The grid is finer near the surface of the cube in all directions and near the plate. In *LES* for getting good results, height of the first cell in near walls should be achieved from $y^+=1$ that y^+ follows as eq. (16)

$$y^+ = \frac{u^* y}{\nu} \quad , \quad u^* = \sqrt{\frac{\tau_0}{\rho}} \quad (16)$$

So in this study we used $y^+=1$ for the first cell in near walls. The minimum grid spacing used in the present computations is 0.019 in x direction, 0.022 in y direction and 0.02 in z direction with a grid expansion ratio of 1.06. The number of grid points used in the present computations were $111 \times 69 \times 105$ in the x, y, z direction, respectively.

The geometry considered in this study consists of a surface-mounted cube with a uniform velocity at the inlet (fig. 1). The streamwise, normal and spanwise lengths of the computational domain are $11H$, $5H$, and $7H$ respectively. The inlet profile was chosen according to the experimental study of Nakamura *et al* [2]. Uniform flow is therefore imposed at the inlet of the computational domain. The free-stream turbulence intensity was about 0.5 per cent. The no-slip boundary conditions were used for all the walls. The outlet boundary condition is of convective type for a quantity ϕ follows as eq. (17).

$$\frac{\partial \phi}{\partial t} + U_b \frac{\partial \phi}{\partial n} = 0 \quad (17)$$

Such convective boundary condition is capable of predicting unsteady flow behaviour at the exit with good accuracy. The spanwise boundary condition was selected symmetry. Surfaces of cube and plate have wall boundary condition. Surfaces of cube and plate were under condition of constant heat flux. The Reynolds number is, $Re = U_{inlet} H / \nu = 31000$ and Prandtl number, $Pr = \nu / \alpha = 0.72$.

3. Results and discussion

When fluid flow passes over a wall mounted cube, variables such as velocity, pressure and etc change and phenomena form around the cube. These phenomena effect on turbulence intensity, convective heat transfer and other fluid flow characteristics. In this study these phenomena and their effects were studied on fluid flow and convective heat transfer.

3.1. Flow structure

Flow over the wall mounted cube has a complex phenomenon such as horse shoe vortex, recirculation zones on the top and rear of the cube which are shown in figure 2 and 3. Fluid pressure increases and fluid velocity decreases in near forward edge on both side and top faces. These changes causes fluid flow separates from cube in these faces. Flow separation forms recirculation zone in near these faces that increases turbulence intensity. With separation of fluid flow in mentioned zones fluid velocity gradually increases until reattach onto near backward edge on both side and top faces. Length of recirculation zone on top face (distance of flow separation to flow reattachment place) is showed by L_3 in figure 2. Flow reattachment on

cube happens on downstream corners of top face and downstream corner of both sides face in upper part. A large separation region develops behind the cube which interacts with the horseshoe vortex. Length of this region is showed with L_1 (Fig. 2). Three dimensional, unsteady and complex circulations in this region increase turbulence intensity. This increase has great effects on flow velocity profiles, Reynolds stress and convective heat transfer.

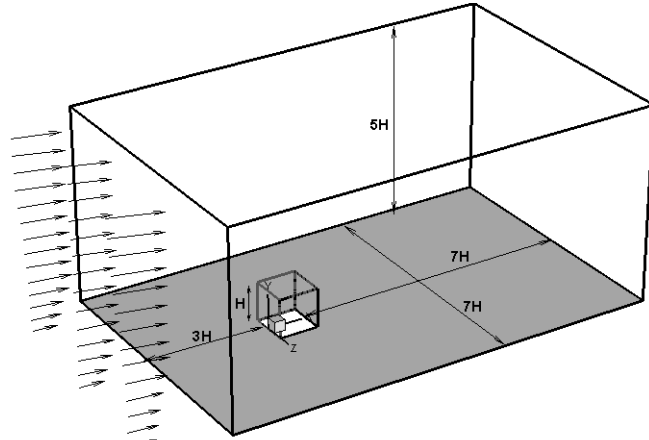


Figure1. Geometry of problem

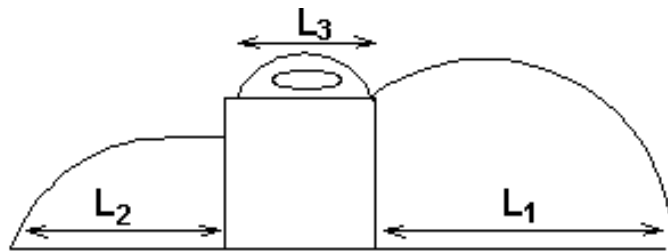


Figure 2.Flow pattern around a wall mounted cube with three vortex lengths.

TABLE 1.VALUES OF THREE VORTEX LENGTHS

Calculation method	L_1	L_2	L_3
Experimental[2]	1.5H	1.04H	.85H
LES(WALE)	1.64H	1.28H	.94H
LES(DS)	1.46H	1.19H	.94H

Figure 4 shows time averaged streamlines on plate ($y=0$) (left) and symmetry plane ($z=0$) (right) for experimental and numerical methods. Numerical simulation is done with *LES* method. *LES* method consists of two subgrid scale models, wall-adapting local eddy viscosity (*WALE*) and dynamic Smagorinsky (*DS*). Figure 2 shows that two *LES* models are able to simulate almost all of phenomena those are mentioned above. Values of three lengths (L_1 , L_2 and L_3) for experiment [2] and numerical simulation results are showed in tab1. The length of large separation region behind and recirculation zone in front of cube, is predicted correctly by *LES* models but L_1 is simulated in good agreement with experiment by *DS* model, while *WALE* model predicted this length somewhat high and *WALE* model predicted L_2 somewhat high toward *DS* model. *LES* models aren't simulated reattachment phenomenon on top and both side faces of cube as well as experiment [2]. All of three dimensional and unsteady phenomena that exist in fluid flow pass on wall mounted cube are showed three dimensionally in fig 4.

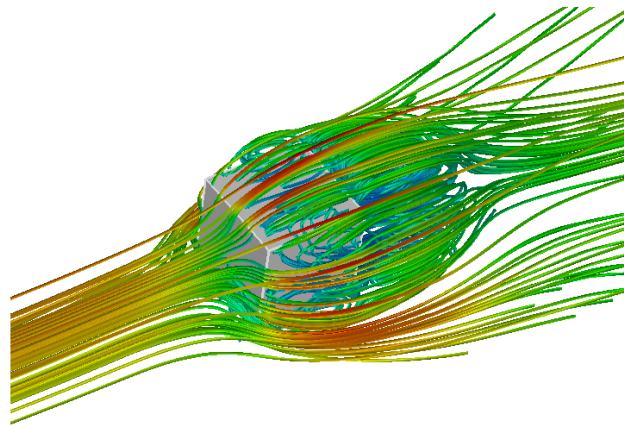


Figure 3. Time averaged streamlines around a wall mounted cube.

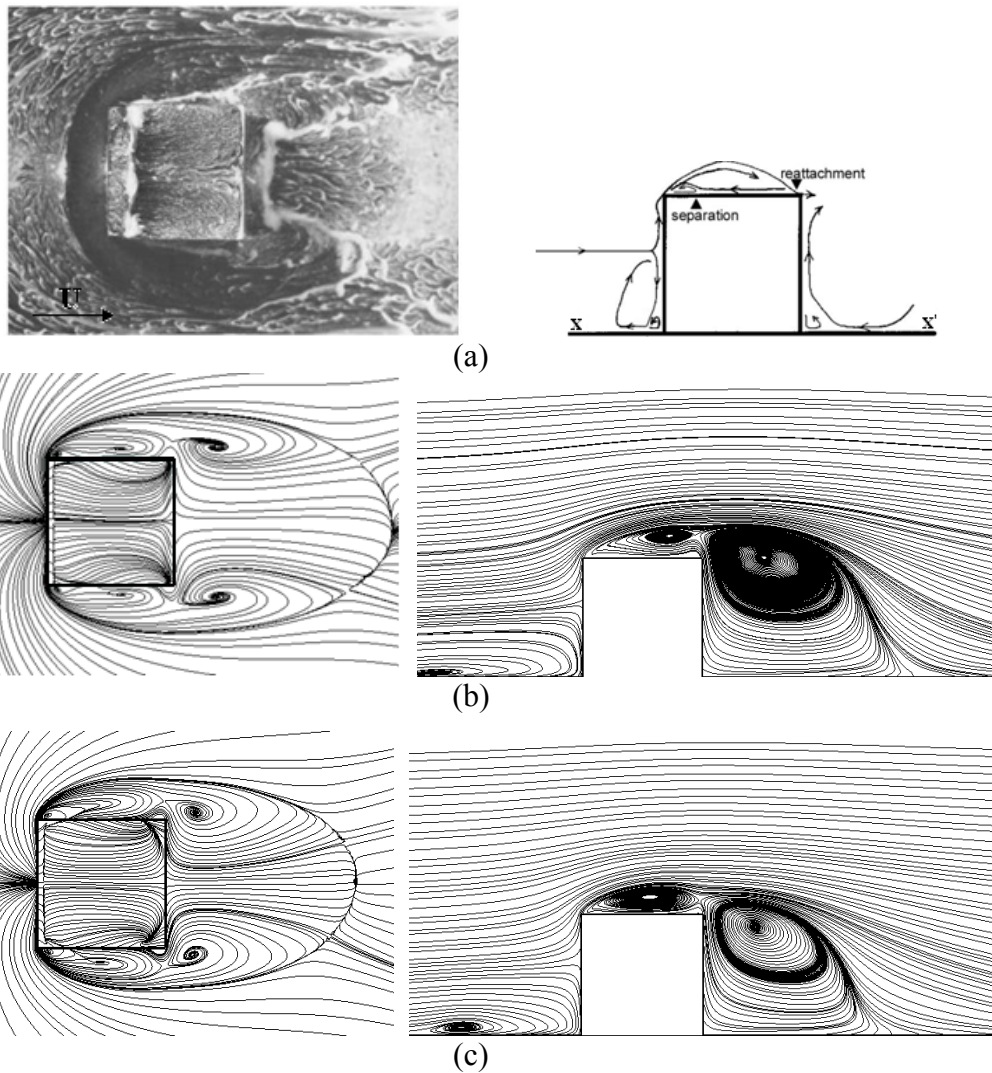


Figure 4. Time averaged streamlines at the floor and centreline of the channel for (a) experimental data [2], (b) WALE and (c) DS models

In the regions of top and behind the cube by formation of complex phenomena and different turbulence intensity, velocity, Reynolds stress and changes of them are different in different positions. In figures 5 and 6, plots of the normalized time averaged streamwise velocity \bar{U}/U_b and the normalized time averaged Reynolds stress $\overline{U'V'}/U_b^2$ are drawn for two *LES* models, in different positions of the behind and top of cube ($x=.5H$, $x=1.5H$, $x=2.5H$, $x=3.5H$) on

symmetry plane ($z=0$). In the separation region behind and top of cube, time averaged streamwise velocity changes, are high that shows the high turbulence intensity in these region. But when distance from cube in behind of it (in x direction) increases, time averaged streamwise velocity changes decrease. Whatever y/H increases to higher than one, time averaged streamwise velocity plots gradient accede to zero and turbulence properties value decrease to zero.

Other fluid flow characteristic that is affected from complex phenomena is Reynolds stress. Changes of Reynolds stress, similar to velocity, in the separation regions behind and top of cube are more than other regions in downstream of cube (fig 6). Because Reynolds stress corresponds with velocity changes. By increasing the distance from the cube in downstream, magnitude of time averaged Reynolds stress decreases. Whatever distance from plate (in vertical direction) increases and flow become free stream, magnitude of Reynolds stress accede to zero. Changes of time averaged streamwise velocity and Reynolds stress in two *LES* models are similar but magnitude of them in two models are different in some positions.

In attention to above points about fluid flow structures, *DS* model simulated flow structures better than *WALE* model. So in this study we used *DS* model for prediction of heat transfer.

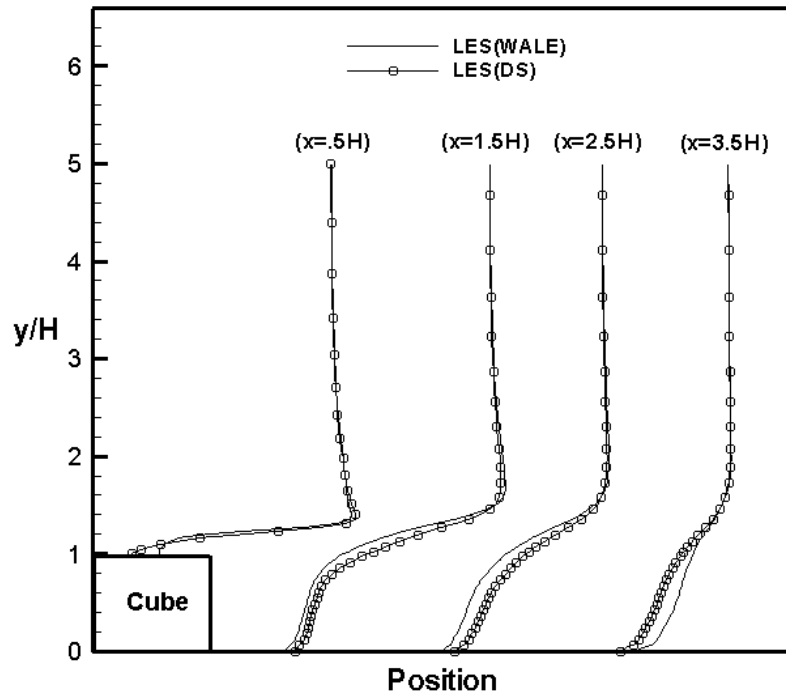


Figure 5. The normalized time averaged streamwise velocity profile (\bar{U}/U_b) at different positions on $Z=0$ plane.

3.2. Heat transfer

Dimensionless mean temperature (T^*) contour over the floor of the channel is plotted in figure 7. Then show local Nusselt number contours in faces of cube and compare it with experimental results [2]. Also for comparison of convective heat transfer in different locations of cube faces, local Nusselt numbers are plotted on $y=0.2H$, $y=0.4H$, $y=0.6H$, $y=0.8H$ and $z=0$, $z=\pm 0.2H$, $z=\pm 0.4H$ faces (the Nusselt number is averaged value between $+z/H$ and $-z/H$).

The horse shoe vortex in the upstream and recirculation region at the rear of the cube make mixing in the flow field, therefore the heat transfer increases in these regions. It can be seen in figure 7 clearly. At the cube sides, two small recirculation regions exist that cause to increase the temperature in these regions in comparison with other area around the cube.

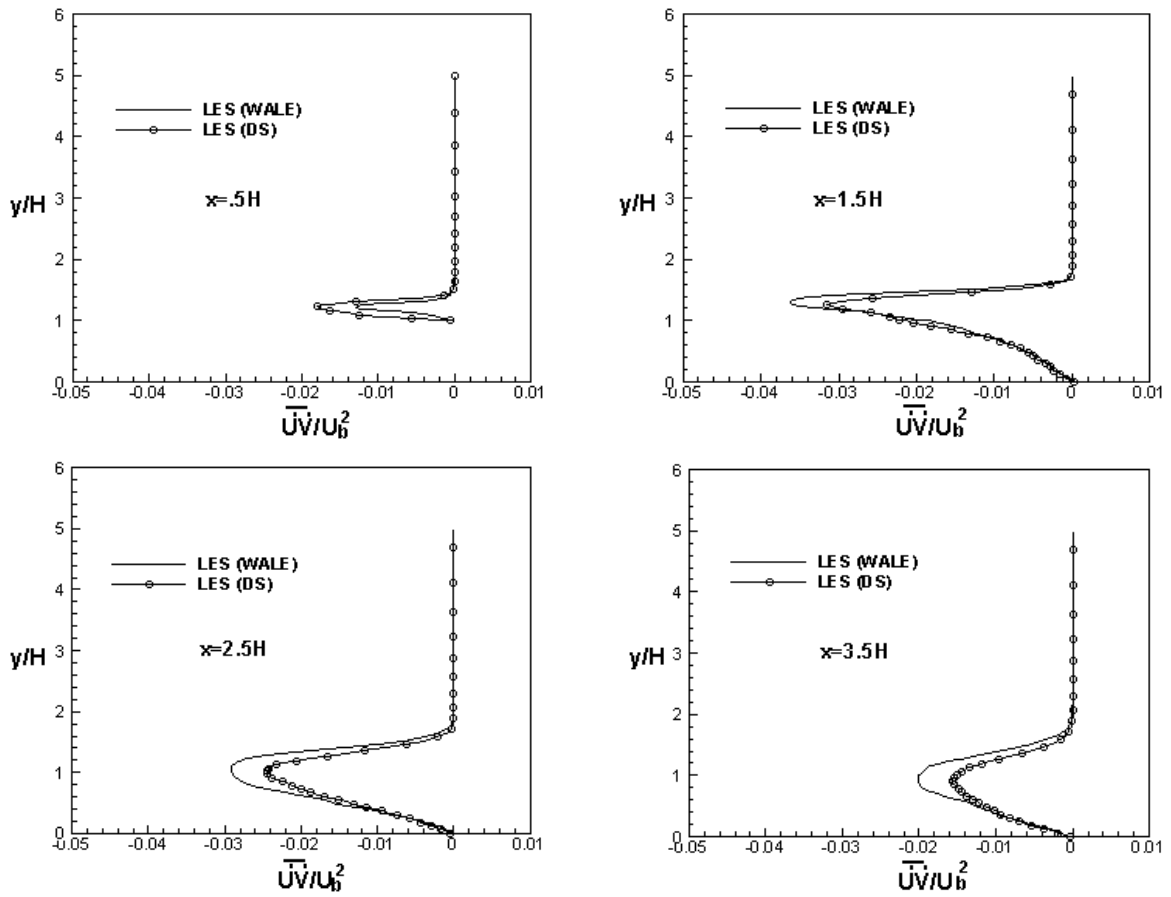


Figure 6. The normalized time averaged Reynolds stress (\overline{UV}/U_b^2) at different positions on $Z=0$ plane.

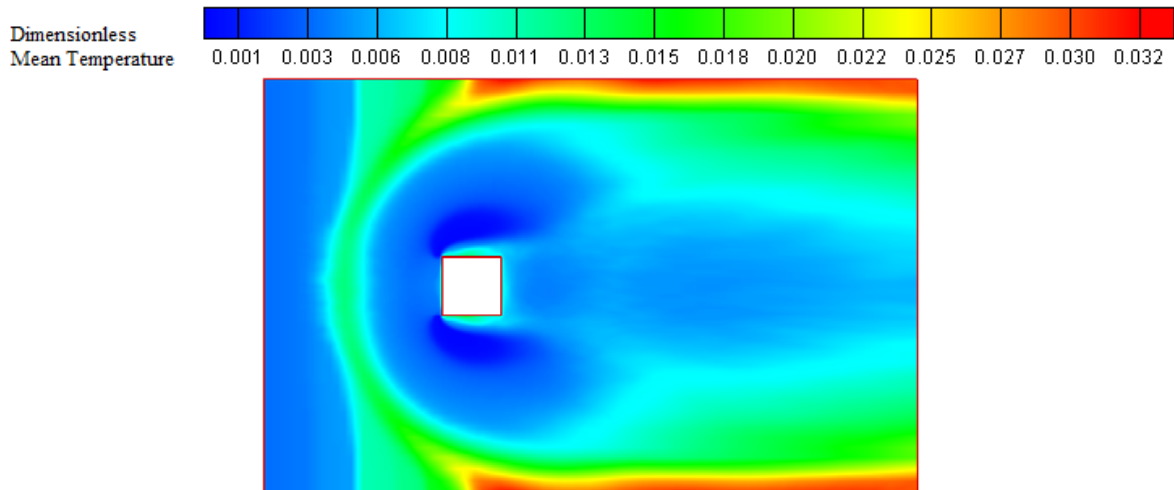


Figure 7. Dimensionless mean temperature contour on the floor of the channel ($y=0$)

Nusselt number is defined as, hH/k , that h , H , k are heat transfer coefficient, cube height and thermal conductivity of fluid respectively. The difference between the temperature of the surface of the cube and the inlet bulk temperature is used to calculate the heat transfer coefficient h as eq. (18).

$$h = \frac{q}{T_s - T_{bi}} \tag{18}$$

Here q , T_s and T_{bi} are the heat flux, the surface temperature and the inlet bulk temperature, respectively.

Figure 8 shows local Nusselt number contour at cube faces for numerical simulation and experimental data [2]. The overall view shows the reasonable accuracy of the numerical simulation in comparison with the experiment [2]. On the front face in stagnation point fluid flow velocity is zero and increases by approaching to edges. So, as we see in figures 8 and 9, convective heat transfer increases approaching to edges and the Nusselt number has maximum value in near edges. We can see in figures 8 and 10 that on the front face the Nusselt number distribution is almost flat along the vertical direction except near the upper and bottom parts. Nusselt number variation, on both side and top faces is higher than other faces. On these faces the Nusselt number at separation and reattachment points has minimum and maximum value respectively and increases from separation to reattachment region. Near the backward edges on both side faces, the values of Nusselt number in the upper part are higher than those in the bottom part. As we mentioned above, *LES* models aren't simulated reattachment phenomenon on top and both side faces of cube as well as experiment [2]. So, as we can see in figure 8, in these regions the experiment Nusselt number value is higher than *LES*. The Nusselt number value on rear face is lower than other faces. Figures 9 and 10 show the local Nusselt number distribution on the rear and front faces. The Nusselt number distribution is almost flat along the horizontal direction except near edges and its values near the side edges are higher than those in central part.

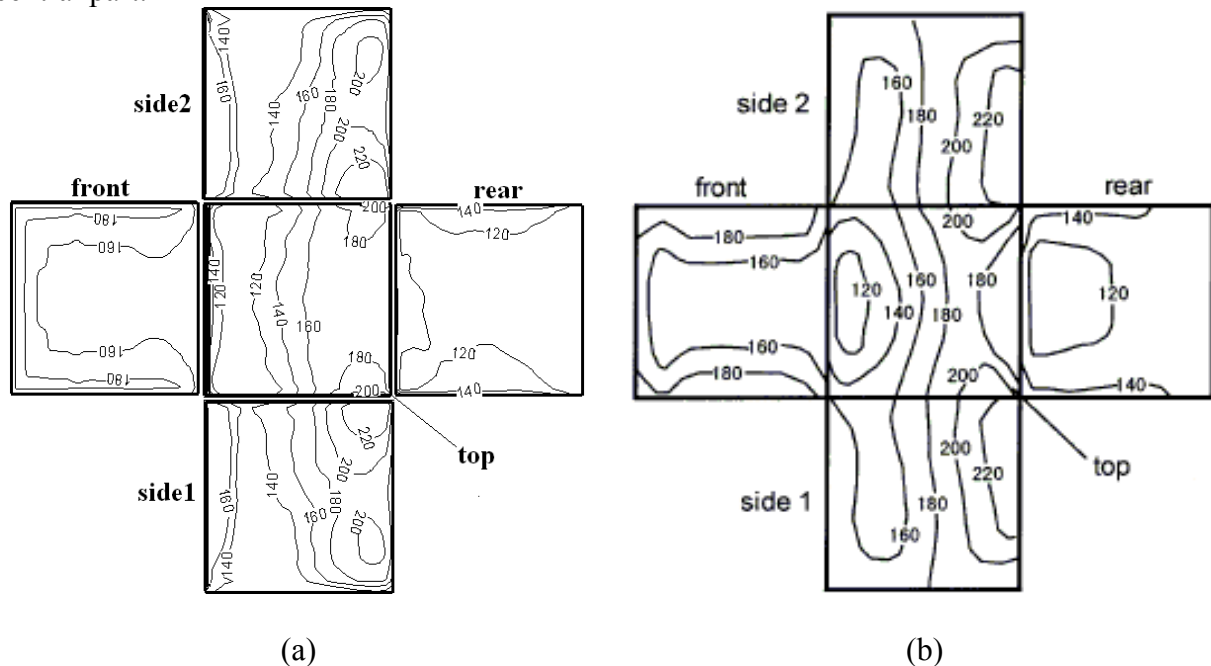


Figure 8. Local Nusselt number contour over the cube surfaces, (a) numerical simulation and (b) experimental data [2].

It is observed that by increasing the y and z , heat transfer rate increases from the cube surfaces. It is due to the separation of the flow from the surfaces of the cube. On both sides and rear faces of the cube this effect is more sensitively. The numerical data shows a reasonable accuracy with the experiment of the Nakamura *et al* [2].

Average Nusselt number at each cube face with the cube overall for experimental and numerical methods is showed in table 2. These values are obtained from the surface-integrated. The value of Nusselt number on the side face is the averaged value of both side faces. Average Nusselt number becomes lower in the order of side, front, top, rear faces. As we mentioned above, *LES* models aren't simulated reattachment phenomenon on both side faces of cube as

well as experiment [2]. So difference of average Nusselt number by experimental result in these faces is higher than other faces.

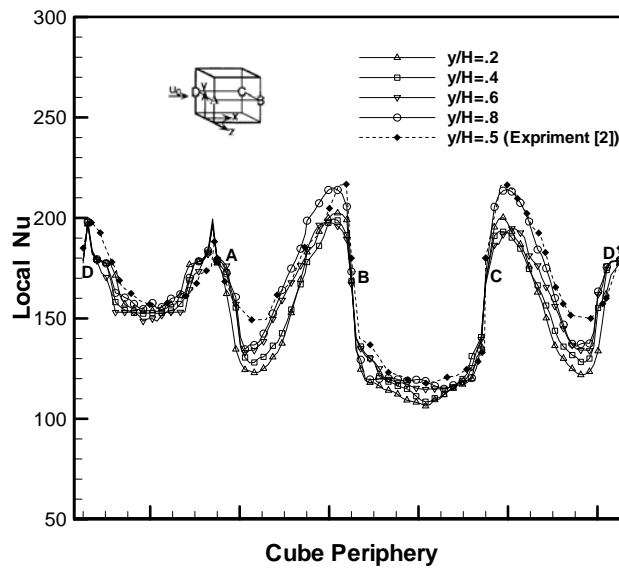


Figure 9. Local Nusselt number distribution around a cube for various heights of y/H .

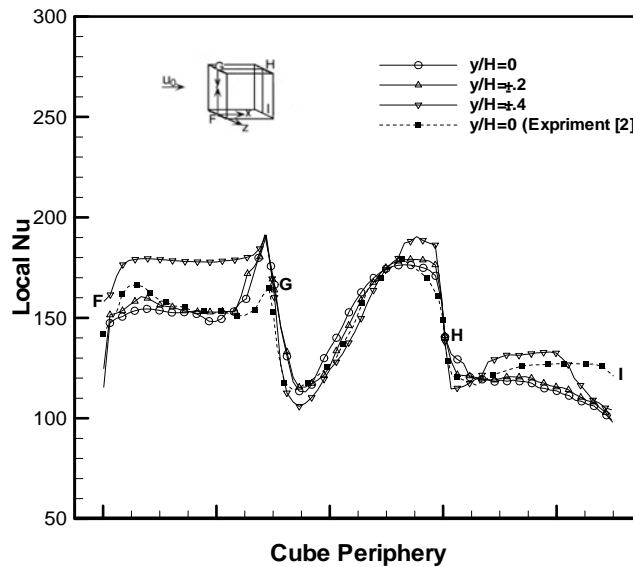


Figure 10. Local Nusselt number distribution around a cube for various z/H

TABLE 2. AVERAGE NUSSLETT NUMBER AT THE CUBE FACES

Faces	Experimental data[2]	present study
Front	153.73	152.51
Side	167.16	164.12
Top	149.58	148.07
Rear	112.36	111.48
Cube	156.32	155.04

4. Conclusion

3D simulation of the flow field and convective heat transfer over a wall mounted cube were done by LES. Comparison of flow parameters with experimental results showed *DS* model has better results toward *WALE* model. Time averaged Reynolds stress and velocity in the separation

regions behind and top of cube are more than other regions. By increasing the distance from the cube at the downstream (in x direction), magnitude of time averaged Reynolds stress decreases.

In horseshoe vortex region on plate, mean temperature decreases. The local convective heat transfer from the surfaces of cube and plate to the fluid is directly related to the complex phenomena. Variation of the Nusselt number, on both side and top faces is higher than other faces. In these faces at separation and reattachment points, local Nusselt number values are minimum and maximum respectively. On the front face the Nusselt number distribution is almost flat along the vertical direction except near the upper and bottom parts. The highest average Nusselt number is obtained for the sides face and the lowest for the rear face.

Nomenclature

C_s	– Smagorinsky constant
C_w	– WALE constant
H	– cube height, [m]
k	– thermal conductivity, [$\text{JK}^{-1}\text{m}^{-1}$]
K	– von karman's constant
h	– heat transfer coefficient, [$\text{Jm}^{-2}\text{K}^{-1}$]
K	– von karman's constant
k	– thermal conductivity, [$\text{JK}^{-1}\text{m}^{-1}$]
Pr	– prandtl number (ν/α)
Pr_t	– turbulent Prandtl number
Nu	– Nusselt number (hH/k)
q	– heat flux, [J]
Re	– Reynolds number ($U_{inlet}H/\nu$)
T_m	– mean temperature, [K]
T_s	– surface temperature, [K]
T_{bi}	– inlet bulk temperature, [K]
T^*	– dimensionless mean temperature ($(T_m - T_{bi})/(qH/k)$)
u^*	– friction velocity, [ms^{-1}]
U_b	– bulk velocity, [ms^{-1}]
U_{inlet}	– velocity at the entrance, [ms^{-1}]
y^+	– normalized distance

Greek Symbols

α	– thermal diffusivity, [m^2s^{-1}]
ν	– kinematic viscosity, [m^2s^{-1}]
ρ	– density, [kgm^{-3}]
δ_{ij}	– kronecker delta
τ_0	– shear stress, [$\text{kgm}^{-1}\text{s}^{-2}$]

References

- [1] Rodi, W. Comparison of LES and RANS calculations of the flow around bluff bodies, *Journal of Wind Engineering and Industrial Aerodynamics*, 69–71, 1997, pp. 55–75.
- [2] Nakamura, H., Igarashi, T and Tsutsui, T. Local heat transfer around a wall mounted cube in the turbulent boundary layer, *Int. J. Heat and Mass Transfer*, 44, 2001, pp. 3385–3395.
- [3] Nakamura, H., Igarashi, T and Tsutsui, T. Local heat transfer around a wall mounted cube at 45° to flow in a turbulent boundary layer. *Int. J. Heat and Fluid Flow*, 24, 2003, pp. 807–815.

- [4] Sohankar, A. Flow over a bluff body from moderate to high Reynolds numbers using large eddy simulation. *Computers & Fluids*, 35, 2006, pp. 1154–1168.
- [5] Niceno, B., Dronkers, A.D.T. and Hanjalic, K. 2002. Turbulent heat transfer from a multi-layer wall-mounted cube matrix: a large eddy simulation. *Int. J. Heat Fluid Flow*, 23, 2002, pp.173– 185.
- [6] Krajnovic, S., Davidson, L. Large eddy simulation of the flow around a bluff body, *AIAA Journal*, 40, 2002, pp. 927-936.
- [7] Farhadi, M., Rahnama, M. Large Eddy Simulation of Separated Flow over a Wall-Mounted cube. *Scientia Iranica*, 13, 2006, pp. 124-133.
- [8] Hwang, J. Y., Yang, K.S. Numerical study of vortical structures around a wall-mounted cubic obstacle in channel flow, *Physics of Fluids*, 16, 2004, pp. 2382-2394.
- [9] Farhadi, M. and Sedighi, K. Three-dimensional study of vortical structure around a cubic bluff body in a channel, *FACTA UNIVERSITATIS Series: Mechanical Engineering*, 4, 2006, pp. 1–16.
- [10] Lammers, P., Jovanovic, J., Durst, F. Numerical experiments on wall turbulence at low Reynolds number, *Thermal Science*, 10, 2006, pp.33-62.
- [11] Bakic, V. Experimental investigation of a flow around a sphere, *Thermal Science*, 8, 2004, pp.63- 81.
- [12] Bakic, V, Schmid, M, Stankovic, B. Experimental investigation of turbulent structures of flow around a sphere, *Thermal Science*, 10, 2006, pp. 97-112.
- [13] Chakrabarty, D, Brahma, R. Effect of wall proximity in fluid flow and heat transfer from a square prism placed inside a wind tunnel, *Thermal Science*, 114, 2007. pp.65-78.
- [14] Nicoud, F, Ducros, F. Subgrid-scale stress modeling based on the square of the velocity gradient tensor, *Flow, Turbulence and Combustion*, 62, 1999, pp. 183–200.
- [15] Germano, M, Piomelli, U, Moin, P, Cabot, W.H. A dynamic subgrid-scale eddy viscosity model, *Phys. Fluids A*, 3, 1991, pp. 1760-1765.
- [16] Lilly, D. K. A Proposed Modification of the Germano Subgrid-Scale Closure Model. *Physics of Fluids*, 4, 1992, pp. 633-635.
- [17] Leonard, B. P. The ULTIMATE conservative difference scheme applied on unsteady one-dimensional advection, *J. Computer Methods in Applied Mech. Eng.*, 88, 1991, pp. 17–74.
- [18] Martinuzzi, R. J and Havel, B. Vortex shedding from two surface-mounted cubes in tandem. *Int. J. Heat Fluid Flow*, 25, 2004, pp. 364–372.
- [19] Farhadi, M and Sedighi, K. Flow over two tandem wall-mounted cubes using large eddy simulation. *Proceedings of the Institution of Mechanical Engineers, Part C: Journal of Mechanical Engineering Science*, 222, 2008, pp. 1465–1475.
- [20] Saim, R, Abboudi, Benyoucef, B. Computational analysis of transient turbulent flow and conjugate heat transfer characteristics in a solar collector panel with internal, rectangular fins and baffles, *Thermal Science*, 14, 2010, pp.221-234.
- [21] Seeta Ratnam, G., Vengadesan, S. Performance of two equation turbulence models for prediction of flow and heat transfer over a wall mounted cube. *Int. J. Heat and Mass Transfer*, 51, 2008. pp. 2834– 2846.
- [22] Hemida, H., Spehr, F., Krajnovic, S. Local heat transfer enhancement around a matrix of wall-mounted cubes using passive flow control: Large-eddy simulations. *Int. J. Heat and Fluid flow*, 29, 2008, pp.1258–1267.
- [23] Rundström, D., Moshfegh, B., 2009. Large-eddy simulation of an impinging jet in a cross-flow on a heated wall-mounted cube. *Int. J. Heat and Mass Transfer*, 52, 2009, pp. 921–931